CrystEngComm

PAPER

View Article Online
View Journal | View Issue

Cite this: *CrystEngComm*, 2015, **17**, 2021

Crystal disassembly and reassembly of heterometallic Ni^{II}–Ta^{V} oxalate compounds†‡

Lidija Androš Dubraja,*[a] Dubravka Matković-Čalogović*[b] and Pavica Planinić*[a]

Four new complexes, $[Ni(bpy)_3]_2[TaO(C_2O_4)_3]Cl{\cdot}11H_2O$ (**1**), $[Ni(bpy)_3]_2[TaO(C_2O_4)_3]Cl{\cdot}12H_2O$ (**2**), $[\{Ni(bpy)_2\}_2(\mu\text{-}C_2O_4)]_{1.5}[TaO(C_2O_4)_3]{\cdot}13H_2O$ (**3**) and $[\{Ni(bpy)_2\}_2(\mu\text{-}C_2O_4)](NO_3)_2{\cdot}H_2C_2O_4$ (**4**) (bpy = 2,2′-bipyridine), have been prepared and investigated by IR spectroscopy and thermal analysis; compounds **1**, **2** and **4** have been characterized by single-crystal X-ray diffraction. In these Ni–Ta oxalate systems the crystal disassembly/reassembly process was observed. Stick-like single crystals of **1** disassemble in the mother liquor and again reassemble to form polyhedral single crystals of **2** having an additional water molecule. Compounds **1** and **2** crystallize in different crystal systems ($P2_1/c$ *vs.* $P2_12_12_1$); nevertheless they exhibit very similar crystal packing of the constituent structural units: the $[Ni(bpy)_3]^{2+}$ cations are involved in a specific intermolecular contact, quadruple aryl embrace (QAE), in a honeycomb 2D hexagonal network, whereas the $[TaO(C_2O_4)_3]^{3-}$ anions and water molecules constitute a 3D hydrogen bonding sublattice. A survey of the Cambridge Structural Database was performed in order to find similar QAE contacts within the crystal structures containing the $[M(bpy)_3]^{n+}$ cation. In a Ni–Ta oxalate system with a different $[\{Ni(bpy)_2\}_2(\mu\text{-}C_2O_4)]^{2+}$ cation environment, compound **3** was obtained. The disassembly/reassembly process occurs in the mother liquor containing crystals of **3**, and after two weeks it yields crystals of **4** with different constituent units: the homodinuclear $[\{Ni(bpy)_2\}_2(\mu\text{-}C_2O_4)]^{2+}$ cation remains unchanged, whereas the (oxalato)tantalate(v) anion decomposes during disassembly of **3** and NO_3^- takes its place as the counteranion in the reassembled crystal form of **4**.

Received 23rd December 2014,
Accepted 26th January 2015

DOI: 10.1039/c4ce02516d

www.rsc.org/crystengcomm

Introduction

In the field of crystal engineering much effort has been devoted to the design and synthesis of novel metal–organic coordination compounds with various combinations of transition metal ions and multifunctional bridging oxalate ligands.[1–8] Various possibilities of coordination, ability to mediate exchange interactions between the metal atoms, and participation in hydrogen bonding are the reasons of such a wide use of oxalate ligands in coordination chemistry.[9] Aromatic N-donor ligands such as 2,2′-bipyridine (bpy) or 1,10-phenanthroline (phen) are also frequently used in crystal engineering, since introduction of a heterocyclic N atom increases the tendency to stack.[10] Interactions between neighbouring aromatic rings are responsible for stabilization of the solid-state structures. Aromatic interactions include three stacking modes: face-centred, off-centre parallel and edge-to-face orientations of the aromatic rings.[11] Another intermolecular motif concerning the interactions between two (or more) molecules with aromatic rings is known as the *molecular aryl embrace*.[12]

In our previous work we have already shown that introduction of complex cations containing N-donor aromatic ligands $[Ni(phen)_3]^{2+}$ to systems with (oxalato)tantalate(v) anions leads to crystallization of stable products of similar chemical compositions but different structural arrangements, depending on the ratio of the reactants and solvents used.[13] We have continued our research on the (oxalato)tantalate(v) anion coordination ability in reactions with nickel(II) salts and bpy ligands, and report herein the heterometallic Ni^{II}–Ta^{V} compounds $[Ni(bpy)_3]_2[TaO(C_2O_4)_3]Cl{\cdot}nH_2O$ [n = 11 (**1**), 12 (**2**)]

[a] *Ruđer Bošković Institute, Bijenička cesta 54, 10000 Zagreb, Croatia. E-mail: Lidija.Andros@irb.hr, planinic@irb.hr*
[b] *Department of Chemistry, Faculty of Science, University of Zagreb, Horvatovac 102a, 10000 Zagreb, Croatia. E-mail: dubravka@chem.pmf.hr*

† Electronic supplementary information (ESI) available: Infrared data for **1**–**4**, X-ray powder diffraction data for the crystal products throughout the whole crystallization process of **1** and **2** (Fig. S1), geometric parameters of the metal coordination spheres in **1**, **2** and **4** (Tables S1, S2 and S4), ORTEP-III drawing of the anion in **1** (Fig. S2), QAE contacts in **2** and in $[P(Ph)_4][Cr(bpy)(C_2O_4)_2]$ (Fig. S3), geometric parameters and graphical representation of hydrogen bonding in **1**, **2** and **4** (Table S3, Fig. S7–S9), geometric parameters and graphical representation of stacking interactions in **4** (Table S5, Fig. S11–S13), the overlay of cation packing in **1** and **2** (Fig. S10), graphical representation of the CSD search for QAE contacts (Fig. S4–S6), the TGA and DTA curves of **1** and **2** measured in synthetic air (Fig. S14 and S15), thermogravimetric data for **1**–**4** (Table S6), and CIF files for **1**, **2** and **4**. CCDC 1026178–1026180. For ESI and crystallographic data in CIF or other electronic format see DOI: 10.1039/c4ce02516d

‡ All authors contributed equally to this work.

and $[\{Ni(bpy)_2\}_2(\mu\text{-}C_2O_4)]_{1.5}[TaO(C_2O_4)_3]\cdot 13H_2O$ (**3**), and one homobinuclear compound $[\{Ni(bpy)_2\}_2(\mu\text{-}C_2O_4)](NO_3)_2\cdot H_2C_2O_4$ (**4**). Scheme 1 shows complex cations and anions in **1** and **3**. In addition to the single crystal X-ray diffraction studies, characterization of the new complexes was accomplished by means of IR spectroscopy and TG/DTA analysis.

Single crystals of **1** and **3** undergo interesting structural transformations that lead to the formation of single crystals of **2** and **4**, respectively. Usually, structural transformations of single crystals in the solutions occur in agreement with the crystal disassembly and reassembly, thus resulting in completely different crystal structures.[14,15] Interestingly, the process of crystal transformation **1** → **2** is accompanied by spontaneous resolution, which converts a racemic compound (**1**) into a racemic conglomerate (**2**). This way of separating enantiomers does not require any optically active auxiliary agent, which makes this method very eligible for the preparation of enantiopure materials.[16,17] Nevertheless, the spontaneous resolution upon crystallization is still a relatively rare phenomenon, as the factors affecting this process are not yet fully clarified.[18] Strong, selective and directional hydrogen bonds were found to promote the homochiral self-assembly of the molecular species.[18,19] Other non-covalent interactions, as well as the presence of different counteranions or solvent molecules, can also influence chiral crystallization.[16–20]

Studies on the structural transformation related to the single crystals of compounds **1** and **3** could open opportunities to gain a better understanding of the fundamental factors that influence crystal nucleation and growth and hence help to develop functional materials.[14]

Results and discussion

Crystal transformations

Although oxalate chemistry of tantalum has been poorly understood so far, studies of this system in reactions with complex cations of nickel(II) have revealed several Ni^{II}–Ta^{V} compounds with different (oxalato)tantalate(V) anions, and interesting structural architectures accomplished by hydrogen bonds and aromatic interactions.[13] Following a simple procedure, similar to the one we used for the preparation of the $[Ni(phen)_3][Ta(L)(C_2O_4)_3]\cdot nH_2O$ [(L, *n*) = (OH^-, 8.5); ($OC_2H_5^-$, 1); (OCH_3^-, 1)] complexes,[13] but using bpy instead of phen ligands, surprisingly, we have isolated only the complexes containing $[TaO(C_2O_4)_3]^{3-}$, the same (oxalato)tantalate species we had observed also in $\{Ba_2(H_2O)_5[TaO(C_2O_4)_3]HC_2O_4\}\cdot H_2O$.[21] From this it is evident that bulky cations, such as $[Ni(phen)_3]^{2+}$ and $[Ni(bpy)_3]^{2+}$, dictate the structural arrangement and also influence changes in the coordination sphere of tantalum. The tendency of Ni^{II}–Ta^{V} oxalate systems with bpy ligands to crystallize with more water molecules is probably due to the existence of more voids in the structures (in relation to similar compounds with phen ligands).

An analogous oxalate anion of niobium(V), in which the niobium atom is doubly bonded to an oxo-oxygen atom, is found in various heterometallic niobium complexes.[22–24] Among them, very similar compounds to the presented tantalum species, *i.e.* $[Ni(bpy)_3]_2[NbO(C_2O_4)_3]Cl\cdot nH_2O$ (*n* = 11, 12), have also been prepared and structurally characterized.[23] A spontaneous process of crystal transformation from one solvatomorph to another was observed when the crystals were left in the solution. The same process takes place with compounds **1** and **2**: if the stick-like monoclinic crystals of **1** (Fig. 1, left) are left to stand in the mother liquor they are transformed to the orthorhombic polyhedral crystals of **2** (Fig. 1, right), containing an additional water molecule. A huge change in the crystal habit indicates disassembly and reassembly of the molecular cations and anions into a new crystal. The metastable crystals of **1** are disassembled over a one-week period and the thermodynamically more stable crystals of **2** are reassembled. Composition of the crystal products was tested by X-ray powder diffraction throughout the whole crystallization process (on the sixth, tenth and fourteenth day of the mother liquor lifetime). During the first week of crystallization only crystals of **1** exist. In the middle of the crystallization period both types of crystals are present in the mother liquor, and after two weeks of mother liquor lifetime **2** is obtained as a phase-pure solid (Fig. S1, ESI†).

Breu *et al.* have described a similar crystal behaviour, wherein the metastable and stable crystal phases appear in the solution-mediated transformation.[25] The metastable compound crystallizes first since its nucleating phase is the one with the lowest free-energy barrier of formation. When the solution concentration is between the solubility of the metastable and the stable form, the stable form precipitates through the dissolution of the less stable form.[25] The thermodynamically controlled crystallization of **2** involves spontaneous resolution of the $[Ni(bpy)_3]^{2+}$ cations.

The crystals of **1** and **2** are stable under atmospheric conditions if they are isolated from the mother liquor (pH ≈ 3.2).

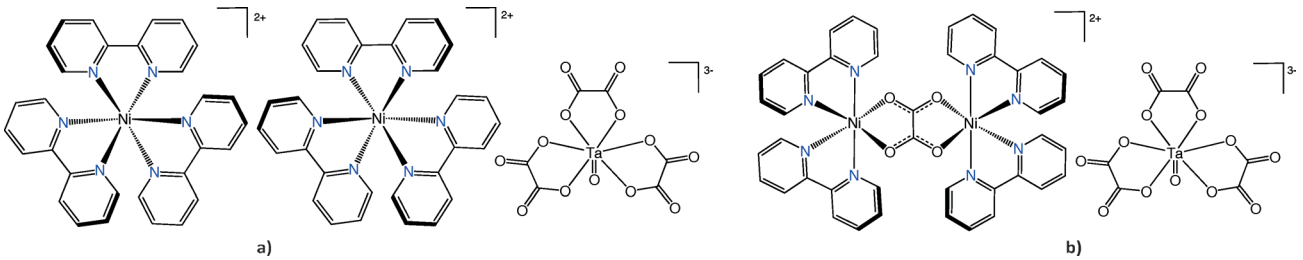

Scheme 1 Complex cations and anion in compounds a) $[Ni(bpy)_3]_2[TaO(C_2O_4)_3]Cl\cdot 11H_2O$ (**1**) and b) $[\{Ni(bpy)_2\}_2(\mu\text{-}C_2O_4)]_{1.5}[TaO(C_2O_4)_3]\cdot 13H_2O$ (**3**).

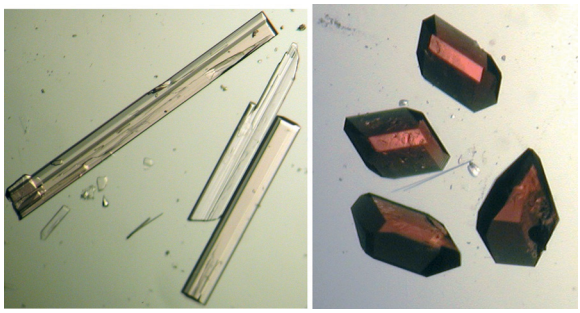

Fig. 1 Microscopic images of the crystals of **1** and **2**, respectively.

If the crystals of **1** are re-suspended in water, crystal transformation **1** → **2** does not occur since during crystal disassembly of **1** in water (pH ≈ 5.6) hydrolysis of the (oxalato)tantalate(v) anion takes place, making reassembly of compound **2** impossible. The hydrolyzed (oxalato)tantalate(v) anion precipitates as an amorphous white sediment. A similar process, which suggests decomposition of molecular components, has been observed during crystal transformation **3** → **4**. Crystals of **3** are very unstable, and that is why satisfactory crystal data could not be collected. However, complex cations and anions are clearly visible in the Fourier electron density map. One and a half bridged $[\{Ni(bpy)_2\}_2(\mu\text{-}C_2O_4)]^{2+}$ units are the cationic part, and the anion is $[TaO(C_2O_4)_3]^{3-}$. After a two-week period crystals of **3** disassemble to the complex cation $[\{Ni(bpy)_2\}_2(\mu\text{-}C_2O_4)]^{2+}$, while the tris(oxalato)oxotantalate(v) anion is hydrolyzed and precipitated. The presence of nitrate counteranions in the mother liquor, together with $[\{Ni(bpy)_2\}_2(\mu\text{-}C_2O_4)]^{2+}$ cations, enables the reassembly of new thicker violet crystals of **4**.

Molecular and crystal structures

Compounds **1** and **2** contain the same constituent structural units: $[Ni(bpy)_3]^{2+}$ cations, $[TaO(C_2O_4)_3]^{3-}$ and Cl^- anions, and crystal water molecules. Two enantiomeric forms of $[Ni(bpy)_3]^{2+}$ cations, Δ and Λ, are present in the crystals of **1**, due to the centrosymmetric character of the monoclinic $P2_1/c$ space group. Compound **2** crystallizes in the non-centrosymmetric $P2_12_12_1$ space group, where only one enantiomer $[Ni(bpy)_3]^{2+}$, Δ or Λ, exists in one crystal; in the crystal selected for the X-ray experiment the Δ-enantiomer was found. The bulk samples of **2** are racemic conglomerates.

Structures of the $[Ni(bpy)_3]^{2+}$ cations in compounds **1** and **2** do not differ significantly. The nickel(II) atom in this cation is coordinated with six nitrogen atoms from three bipyridine molecules. Bond distances between the nickel and nitrogen atoms are in the range of 2.072(4)–2.103(4) Å (2.085 Å on average) and are in good agreement with those in the previously described $[Ni(bpy)_3]^{2+}$ cations found in the CSD (average value, 2.085 Å).[26] The six nitrogen atoms are coupled into three pairs and displaced from the ideal octahedral position, leading to a trigonal distortion of the octahedral environment around the nickel atom. The values of the N–M–N angles where the nitrogen atoms belong to the same bipyridine molecule are in the range of 78.38(16)–79.45(15)° (average, 78.82°). The values of the *cis* (*β*) and *trans* (*γ*) N–M–N angles where the nitrogen atoms belong to different bpy ligands are in the ranges of 90.15(18)–95.98(16)° (93.97° on average) and 168.32(17)–172.34(19)° (170.48° on average), respectively. Selected bond lengths and angles in the complex cations of nickel(II) for both compounds are given in Table S1 (ESI†).

The coordination polyhedron around tantalum(v) in the $[TaO(C_2O_4)_3]^{3-}$ anion (Fig. S2, ESI†) is a distorted pentagonal bipyramid formed by one oxo-oxygen atom in the axial position, one oxalate ligand coordinating in both axial and equatorial positions and the other two oxalate ligands in the equatorial position. Deviation of the coordination polyhedron is larger in compound **1**, as can be observed from the value of the angle between two oxygen atoms in the axial position (O1–Ta1–O2) [166.06(17)° in **1**, 170.42(13)° in **2**, ideal value, 180°]. Compared to some other tantalum(v) coordination polyhedra with a similar geometry, where the steric interference is more pronounced, this angle deviates even more.[13] The length of the Ta=O double bond is 1.742(4) Å in **1** and 1.741(3) Å in **2**, which is in good agreement with the Ta=O bond length [1.748(5) Å] in $\{Ba_2(H_2O)_5[TaO(C_2O_4)_3]\text{-}HC_2O_4\}\cdot H_2O$.[21] The length of the Nb=O double bond [1.722(2) Å] in $[Ni(bpy)_3]_2[NbO(C_2O_4)_3]Cl\cdot 12H_2O$ is slightly shorter.[23] The interatomic Ta–O(oxalate) distances are in the range of 2.086(4)–2.197(3) Å (average, 2.124 Å; average for the Ba–Ta compound, 2.133 Å). Table S2 (ESI†) contains selected bond distances and angles of the $[TaO(C_2O_4)_3]^{3-}$ anions in **1** and **2**.

The crystal structures of **1** and **2** are dominated by the interactions between the aromatic ligands known as the *quadruple aryl embrace* – QAE contacts.[23,27] This intermolecular motif consists of two $[Ni(bpy)_3]^{2+}$ molecules with bpy ligands oriented in a way that one pyridyl ring (C_5H_4N) in a two molecule set could direct its edge to the face of the pyridyl ring of the other molecule, forming a cycle of four *edge-to-face* intermolecular interactions, also denoted as $(EF)_4$.[12] Each pyridyl ring functions both as a donor (at the edge) and as an acceptor (at the face) in the $(EF)_4$ motif.[28] Because of the octahedral stereochemistry of the $[Ni(bpy)_3]^{2+}$ cations, the pyridyl groups in compounds **1** and **2** exhibit a less orthogonal arrangement than, for example, phenyl groups in the $[P(Ph)_4]^+$ entities (Fig. S3, ESI†). The angles between two relevant N–Ni–N planes are given in Table 1. There are two symmetry independent $[Ni(bpy)_3]^{2+}$ cations in the unit cells of **1** and **2** (highlighted in blue and green in Fig. 2). One cation has three neighbouring cations: two symmetry independent cations and one symmetry equivalent cation. There are three types of QAE contacts as well: QAE(i) contact between symmetry independent cations, QAE(ii) and QAE(iii) between symmetry equivalent cations. Fig. 2 shows how this type of interaction is spread in two dimensions, forming a honeycomb hexagonal network. Fig. S10 in the ESI† shows that the honeycomb hexagonal cation networks in **1** and **2** are very similar. The only significant difference in the crystal packing of the cations is that in **1** there are two types of honeycomb

Table 1 Geometric parameters of the QAE contacts for compounds **1** and **2**

Comp.	QAE	Angle between the two relevant intramolecular N–M–N planes for the pair of embracing cations/°	Angle between the planes of aryl rings in contact/°	∠(C_{distal}[a] –Ni···Ni)/°	Ni···Ni/Å
1	(i)	85.40	58.74, 68.97, 50.13, 56.35	165.53	8.310
	(ii)	86.29	44.77, 61.95, 47.63, 61.09	168.01	7.729
	(iii)	89.58	70.84, 55.90, 69.42, 28.89	167.33	7.776
2	(i)	87.49	57.92, 58.67, 46.29, 39.03	167.46	7.467
	(ii)	84.26	57.28, 43.75, 73.04, 56.72	172.98	8.337
	(iii)	80.62	44.53, 78.07, 55.55, 54.82	166.15	8.265

[a] C_{distal} = carbon atom in the bpy molecule which gives the largest C_{distal}–M···M angle.

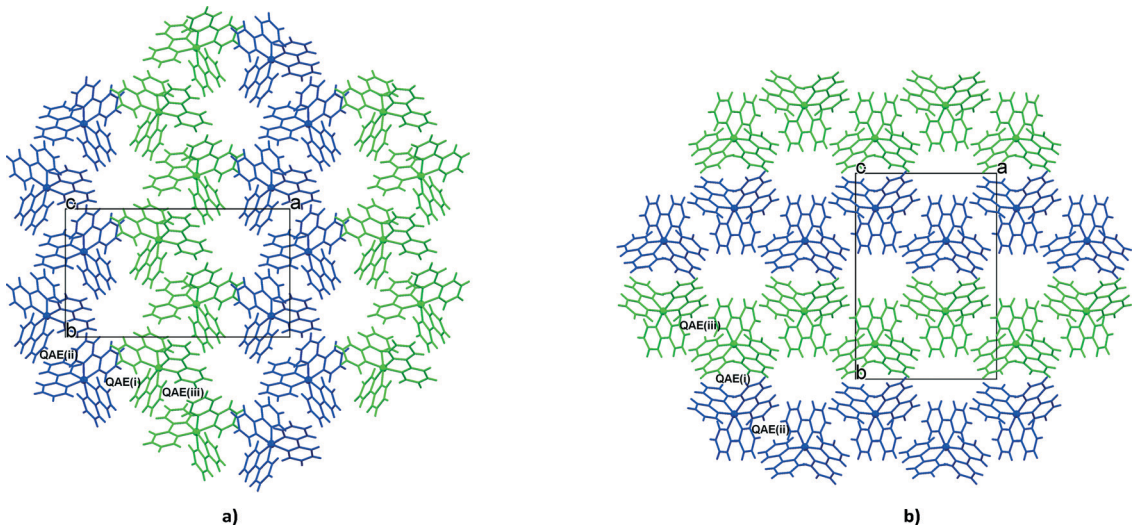

Fig. 2 QAE interactions between $[Ni(bpy)_3]^{2+}$ cations in a) **1** and b) **2**. The symmetry equivalent cations are shown in blue and green.

hexagonal layers; one is formed of Δ-cations and another of Λ-cations, while in **2** all cations are Δ-enantiomers. Table 1 contains additional structural parameters that describe the QAE contacts: angles between the least-square planes of the pyridyl rings involved in the contact, angles between C_{distal}–Ni···Ni (C_{distal} defined as the carbon atom which gives the largest C_{distal}–Ni···Ni angle), and the distances between two Ni atoms of two QAE-connected cations. For example, in the structures containing $[As(Ph)_4]^+$ cations, the contacts comprising a total of four phenyl rings in the interaction domain are usually recognized by C_{distal}–As···As angles in the range of 140–167°, and the As···As distances are lower than 9 Å.[29] Also, the edge of one phenyl ring is inclined at about 60° to the face of another ring.[30] In compounds **1** and **2**, C_{distal}–Ni···Ni angles and Ni···Ni distances are within the specified range, whereas the inclination between pyridyl rings deviates more in comparison to the $[As(Ph)_4]^+$ cations.

In order to get better insight into the orthogonal quadruple aryl embraces between the $[M(bpy)_3]^{n+}$ cations, a search of the Cambridge Structural Database (CSD) was performed.[26] The search was limited to the cations of transition metal ions with the intermolecular distance between metal ions <9.5 Å. Only compounds with an orthogonal $[M(bpy)_3]^{n+}$ cation arrangement were analysed (with the angle between the two relevant N–M–N planes for the pair of embracing cations above 80°).

Limitations were also used for the C_{distal}–M···M angle (140–173°) and the inclination between two pyridyl rings in contact (above 28°). According to the above criteria 164 structures were found in the CSD. The largest number of structures has a C_{distal}–M···M angle value in the range of 164–168°, with the inclination between two pyridyl rings in contact in the range of 55–61°. The average M···M value was found to be 8.035 Å. Graphical representation of the CSD search is given in the ESI† (Fig. S4–S6).

The anions and crystallization water molecules in **1** and **2** are located between the $[Ni(bpy)_3]^{2+}$ cations assembled by the supramolecular QAE contacts. Fig. 3 shows anions and crystallization water molecules connected through hydrogen bonds in a 2D hydrogen bonding network. In **1** the hydrophilic layers are composed of two alternating ladder-like motifs, one containing $[TaO(C_2O_4)_3]^{3-}$ anions and water molecules, and the other containing chlorine anions and water molecules (Fig. 3a). In **2** both types of anions are surrounded by water molecules and alternately appear throughout the hydrophilic layer (Fig. 3b). Water molecules O15 and O16 in **1** (water molecule O17 in **2**) are located inside the hydrophobic layer, in the honeycomb cavities (Fig. 2). These water

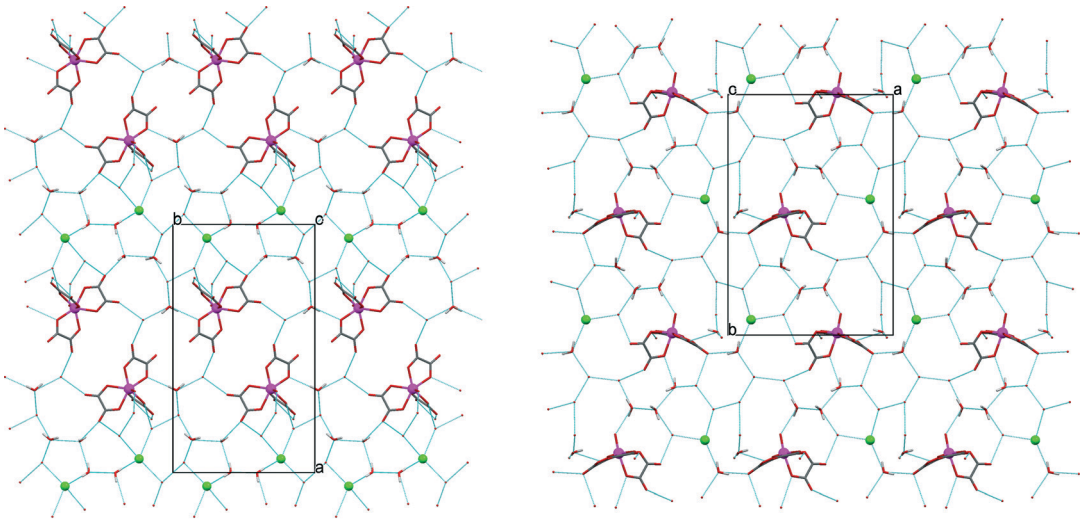

Fig. 3 The hydrophilic layer in the crystal packing of a) **1** and b) **2**. Tantalum atoms (violet) and chlorine atoms (green) are depicted in ball representation.

molecules are involved in hydrogen bonds with $[TaO(C_2O_4)_3]^{3-}$ anions, extending/connecting the hydrophilic layers into a three-dimensional hydrogen bonding sublattice (Fig. S7 and S8, ESI†). The $[TaO(C_2O_4)_3]^{3-}$ anions are oriented in a different manner in **1** and **2**; in **1** the oxo ligand and one oxalate group participate in hydrogen bonds with water molecules inside the hydrophobic cavity, while the other two oxalate groups are involved in hydrogen bonds within the hydrophilic layer. In **1** the arrangement of ligands is inverted (Fig. 3). Geometric parameters describing the hydrogen bonding scheme are given in Table S3 in the ESI.† An overlay of the hydrogen bonding sublattices in **1** and **2** is shown in Fig. S9 in the ESI.†

From the comparison of the anion positions in **1** and **2**, it is evident that the anions in **2** are more distant from each other and the water molecules more effectively solvate and separate them, thus decreasing electrostatic repulsion. Moreover, it is interesting to note that **1**, although having one water molecule less than **2**, has two water molecules placed inside the hydrophobic cavity, while in the same cavity of **2** there is only one water molecule. The differences in crystal packing of cations are minor. Therefore, based on the differences observed in the hydrogen bonding pattern, it can be concluded that hydrogen bonds to a larger extent stabilize the crystal structure of compound **2**. In light of that information hydrogen bonding can be considered as one of the driving forces for crystal transformation **1** → **2**, as well as for the spontaneous resolution that follows this transformation.

The asymmetric unit of **4** contains one oxalate-bridged $[\{Ni(bpy)_2\}_2(C_2O_4)]^{2+}$ cation, two NO_3^- anions and two crystallographically independent oxalic acid molecules in which the midpoint of the C–C bond is located in the inversion centre (Fig. 4). Coordination geometries of the nickel cations (selected bond distances and angles) are given in the ESI† (Table S4). Two nickel cations are separated by 5.383 Å. The overall structural arrangement is driven by aromatic stacking interactions that are spread in three dimensions (Fig. S11–S13 in the ESI†). Hydrogen bonds are present between hydrogen atoms of the oxalic acid molecules and NO_3^- anions. The parameters describing the crystal packing contacts are given in the ESI† (Tables S3 and S5).

Infrared spectroscopy

The IR spectra of the prepared complexes are in agreement with the results of the X-ray analysis: the presence of chelating, bidentate and bis(bidentate) oxalate groups, 2,2′-bipyridine ligands and water molecules is inferred from the spectra.[31] All absorption bands observed in the IR spectra of **1**–**4** are

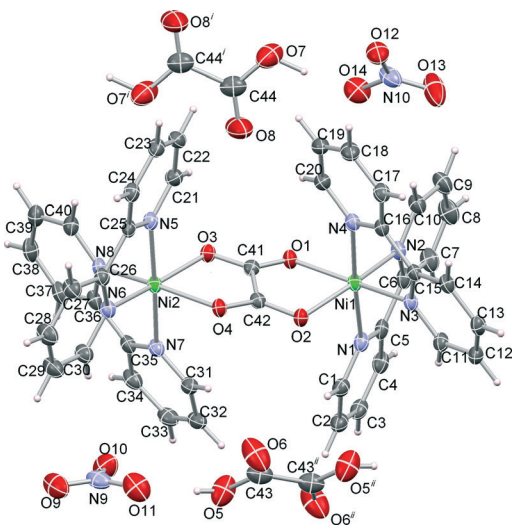

Fig. 4 ORTEP-III drawing of **4**, with the atom-numbering scheme. Displacement ellipsoids are drawn at the 50% probability level and hydrogen atoms are depicted as spheres of arbitrary radii. Symmetry operators: (i) –*x*, –*y*, 2 – *z*; (ii) 1 – *x*, 1 – *y*, 1 – *z*.

given in the ESI.† The absorption bands of medium intensity found in the 3600–3200 cm^{-1} region originate from the O–H stretching vibration [ν(OH)] of crystallization water molecules or oxalic acid molecules (in **4**). Other oxalic acid stretching vibrations are observed in the spectrum of **4** at 1718 and 1267 cm^{-1}. The strong band also present in the spectrum of **4** at 1385 cm^{-1} is due to the stretching vibrations of the nitrate group [ν(NO)]. Stretching vibration of the C–O bond from the bridging oxalate ligand in compounds **3** and **4** could be recognized as a very strong absorption band located at 1638 cm^{-1}. The absorption bands corresponding to the oxalate groups coordinated to tantalum(v) and stretching vibrations of the Ta═O double bond for compounds **1–3** are summarized in Table 2.

Thermal analysis of compounds 1–4

Simultaneous TG and DTA analyses of compounds **1–4** were carried out in a stream of synthetic air. The data obtained from the thermal analysis are supported by the chemical and X-ray diffraction analysis. The TG and DTA curves of compounds **3** and **4** are presented in Fig. 5 and the thermogravimetric data are summarized in Table S6 in the ESI.†

The character of thermal decomposition for compounds **1** and **2** is almost identical (TG and DTA curves are given in Fig. S14 and S15 in the ESI†). The loss of water molecules in these two compounds is accompanied by a broad DTA minimum in the temperature range of 45–170 °C. Another DTA peak at 182 °C indicates the chlorine gas release. In both compounds the elimination of six bpy molecules ends at approximately 460 °C, but this process partly overlaps with the next process – decomposition of the three oxalate ligands. The two processes may be distinguished on the derived DTA curves. Decomposition of the compounds slows down at ~600 °C and there is no major change in mass with further heating up to 1000 °C. The thermal decomposition residue in both compounds is a mixture of oxides NiO and $NiTa_2O_5$ (exp. 21.08%, calcd 21.17% for **1**, exp. 20.55%, calcd 20.96% for **2**).

The loss of water molecules in **3** occurs in two steps and is characterized by weak endothermic effects. The TG analysis indicates 13 crystallization water molecules. The largest decrease in mass occurs in the temperature range of 300–400 °C, when decomposition of six bpy and four and a half oxalate molecules takes place. These two processes overlap, but several peaks can be distinguished on the DTA curve (Table S6, ESI†). The thermal decomposition product of **3** at 800 °C corresponds to the mixture of oxides NiO and $NiTa_2O_5$ (exp. 22.88%, calcd 22.93%).

Homometallic compound **4** is more stable than compounds **1–3** when the temperature increases above room temperature, because there are no crystallization water molecules in its structure. The oxalic acid molecule starts to decompose at 120 °C. Four more steps of decomposition can be observed on the TG curve, corresponding to the nitrate, bpy and oxalate release. The final breakdown of the aromatic ring is accompanied by two strong peaks on the DTA curve (400, 406 °C). In the final step (Table S6, ESI†) the bridging oxalate group decomposes to gaseous CO, while two O atoms are retained in the product of the thermal decomposition, NiO (exp. 14.26%, calcd 14.30%).

Table 2 Selected absorption bands in the IR spectra of compounds **1–3**

	Bidentate oxalate group				
	ν_{as}(CO)	ν_{s}(CO)	δ(OCO)	ν(Ta–O)	ν(Ta═O)
1	1731, 1714, 1692	1384, 1249	800	550	905, 892
2	1731, 1712, 1688	1392, 1248	803	550	908, 887
3	1721, 1693	1357, 1250	806	555	908, 882

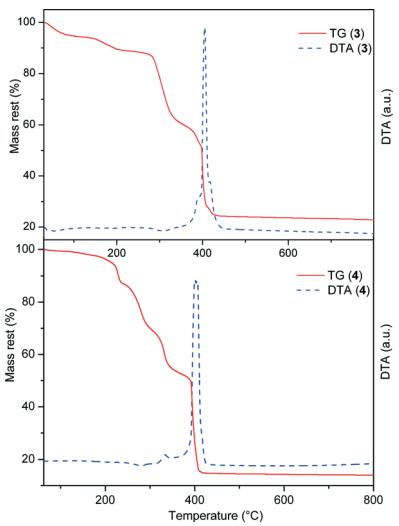

Fig. 5 The TG and DTA curves for compounds **3** and **4** measured in a synthetic air atmosphere.

Conclusions

A very interesting process of crystal disassembly/reassembly was observed for two new Ni–Ta complex species, **1** and **3**. This process yielded two new crystal forms, **2** and **4**. The two crystal transformation processes, **1** → **2** and **3** → **4**, are very different in nature. During transformation process **1** → **2** all constituent structural units reassemble into a new compound; the chemical composition of compounds **1** and **2** differs only by the number of crystallization water molecules (11 *vs.* 12). The formation of **4**, on the other hand, requires the presence of NO_3^- counteranions, because disassembly of **3** causes hydrolysis of the tris(oxalato)oxotantalate(v) anions. The crystals of **3** are very unstable, and this is the reason for the poor X-ray diffraction data.

Crystal transformation **1** → **2** is followed by a spontaneous separation of racemic compound **1**, containing both Δ- and Λ-$[Ni(bpy)_3]^{2+}$ cations, into racemic conglomerates of both enantiomers (Δ or Λ). Analysis of the crystal packing of **1** and **2** showed very similar two-dimensional honeycomb hexagonal networks of the QAE connected cations, whereas the hydrogen bonding scheme revealed significant differences. On the

Table 3 Crystallographic data and structural refinement details for the compounds $[Ni(bpy)_3]_2[TaO(C_2O_4)_3]Cl{\cdot}11H_2O$ (**1**), $[Ni(bpy)_3]_2[TaO(C_2O_4)_3]Cl{\cdot}12H_2O$ (**2**), and $[\{Ni(bpy)_2\}_2(\mu\text{-}C_2O_4)](NO_3)_2{\cdot}H_2C_2O_4$ (**4**)

Compound	**1**	**2**	**4**
Empirical formula	$C_{66}H_{70}Ni_2TaClN_{12}O_{24}$	$C_{66}H_{72}Ni_2TaClN_{12}O_{25}$	$C_{44}H_{34}Ni_2N_{10}O_{14}$
Formula weight/g mol^{-1}	1749.12	1767.14	1044.23
Crystal colour, habit	Pink, stick	Pink, polyhedron	Violet, stick
T/K	293(2)	293(2)	150(2)
Crystal system	Monoclinic	Orthorhombic	Triclinic
Space group	$P2_1/c$	$P2_12_12_1$	$P\bar{1}$
a/Å	23.8900 (3)	14.9775(2)	9.2921(3)
b/Å	13.37190(10)	21.8439(2)	12.8702(3)
c/Å	23.1855(3)	22.3074(3)	18.9812(5)
α/°	90	90	84.660(2)
β/°	101.2320(10)	90	75.969(2)
γ/°	90	90	85.056(2)
V/Å^3	7264.85(14)	7298.25(15)	2187.94(10)
Z	4	4	2
ρ_{calcd}/g cm^{-3}	1.594	1.595	1.585
μ/mm^{-1}	4.383	2.130	1.781
F(000)	3512	3536	1072
Crystal size/mm^3	0.35 × 0.07 × 0.05	0.35 × 0.25 × 0.14	0.30 × 0.10 × 0.08
θ range/°	3.77–65	4.29–28.97	3.46–75.90
No. of measured reflections	39 712	28 831	21 122
No. of independent reflections	12 352	16 073	8978
No. of observed reflections	11 711	13 045	7735
No. of parameters, restraints	999, 18	998, 16	639, 0
R_{int}	0.0313	0.0272	0.0428
R^a, wR^b [$I > 2\sigma(I)$]	0.0500, 0.1406	0.0360, 0.0774	0.0432, 0.1218
R, wR [all data]	0.0517, 0.1419	0.0470, 0.0793	0.0509, 0.1352
Flack param.,[41] conf.	—	−0.008(5), Δ	—
Goodness of fit, S^c	1.093	0.965	1.059
$\Delta\rho_{max}$, $\Delta\rho_{min}$/e Å^{-3}	0.934, −2.032	1.801, −0.949	0.687, −0.594

^{a} $R = \sum||F_o| - |F_c||/\sum|F_o|$. ^{b} $wR = [\sum(F_o^2 - F_c^2)/\sum w(F_o^2)^2]^{1/2}$. ^{c} $S = \sum[w(F_o^2 - F_c^2)^2/(N_{obs} - N_{param})]^{1/2}$.

basis of the performed experiments and the crystal structures, it can be concluded that crystal transformation **1** → **2** is solution mediated. Moreover, the homochiral self-assembly of cations is obviously governed by hydrogen bonds that form a chiral environment for the cations.

Experimental

Materials and physical measurements

The (oxalato)tantalate(v) solution was prepared by dissolving freshly precipitated $Ta_2O_5{\cdot}nH_2O$ in an aqueous solution of $H_2C_2O_4{\cdot}2H_2O$, following the procedure described previously.[32] All other chemical reagents used in the synthesis were purchased from commercial sources and applied without further purification. The tantalum content in the solution was determined in the form of Ta_2O_5. Elemental analyses for C, H and N in **1**–**4** were carried out using a Perkin Elmer Model 2400 microanalytical analyser. Infrared spectra were recorded with KBr pellets using a Bruker Alpha-T spectrometer in the 4000–350 cm^{-1} range. Thermal analysis was performed with a Shimadzu DTG-60H analyser, in the range from room temperature to 1000 °C, in a stream of synthetic air at a heating rate of 10 °C min^{-1}.

Synthesis of $[Ni(bpy)_3]_2[TaO(C_2O_4)_3]Cl{\cdot}11H_2O$ (1). The compound $[Ni(bpy)_3]Cl_2{\cdot}6H_2O$ (282.49 mg, 0.4 mmol) was dissolved in 10 mL of water. Then the (oxalato)tantalate(v) solution (2 mL) [m(Ta) = 36.2 mg, 0.2 mmol] was added dropwise with stirring, and the reaction mixture was additionally stirred for 30 minutes. A small amount of a white precipitate that immediately appeared was removed by filtration after stirring. In the next 24 hours, pink stick-like crystals of $[Ni(bpy)_3]_2[TaO(C_2O_4)_3]Cl{\cdot}11H_2O$ (**1**) started to appear. The crystallization of **1** lasted over the next five days.

Synthesis of $[Ni(bpy)_3]_2[TaO(C_2O_4)_3]Cl{\cdot}12H_2O$ (2). If the crystals of **1** are left to stand in the mother liquor in a closed beaker at room temperature, after one week their number starts to decrease, while another kind of polyhedral crystal starts to form. Structural analysis of polyhedral crystals showed that their composition corresponds to the formula $[Ni(bpy)_3]_2[TaO(C_2O_4)_3]Cl{\cdot}12H_2O$. After a total of two weeks there were no more stick-like crystals of **1**, only polyhedral crystals of **2**.

Synthesis of $[\{Ni(bpy)_2\}_2(\mu\text{-}C_2O_4)]_{1.5}[TaO(C_2O_4)_3]{\cdot}13H_2O$ (3). An aqueous solution (8 mL) of $Ni(NO_3)_2{\cdot}6H_2O$ (87.2 mg, 0.3 mmol) was stirred with an ethanol solution (2 mL) of bpy (93.7 mg, 0.6 mmol) for 15 minutes. After that the (oxalato)tantalate(v) solution (1 mL) [m(Ta) = 18.1 mg, 0.1 mmol] was added dropwise to the mixture and the stirring was continued for 15 more minutes. A small amount of a blue precipitate that formed during the stirring was

removed by filtration. Within a three-day period, violet stick-like crystals of **3** formed. Found, %: C, 43.23; H, 4.33; N, 9.01. Calcd for $C_{69}H_{74}Ni_3TaN_{12}O_{32}$, %: C, 42.71; H, 3.84; N, 8.66.

Synthesis of $[\{Ni(bpy)_2\}_2(\mu\text{-}C_2O_4)](NO_3)_2\cdot H_2C_2O_4$ (4). If the crystals of **3** are left to stand in the mother liquor for more than two weeks in a closed beaker at room temperature, the formation of thicker violet stick-like crystals and a white precipitate can be observed. Structural analysis of the thicker violet stick-like crystals showed that their composition corresponds to the formula $[\{Ni(bpy)_2\}_2(\mu\text{-}C_2O_4)](NO_3)_2\cdot H_2C_2O_4$ (**4**). Found, %: C, 51.23; H, 3.33; N, 14.12. Calcd for $C_{44}H_{34}Ni_2N_{10}O_{14}$, %: C, 50.61; H, 3.28; N, 13.41.

X-ray crystallographic study

The X-ray data for single crystals of **2** and **3** were collected by ω-scans using an Oxford Diffraction Xcalibur 3 CCD diffractometer with graphite-monochromated Mo-Kα radiation (λ = 0.71073 Å). Due to the small size of crystals of **1** and **4** the X-ray data were collected by ω-scans using an Oxford Diffraction Xcalibur Nova R diffractometer with mirror monochromated Cu-Kα radiation (λ = 1.54179 Å, microfocus tube, CCD detector). The measured intensity data were reduced using the CrysAlis[33] software package. The multi-scan absorption correction was applied. The crystal data, experimental conditions and final refinement parameters are summarized in Table 3.

Molecular and crystal structures were solved by direct methods using the program SIR92[34] and refined by the full-matrix least-squares method based on F^2 with anisotropic displacement parameters for all non-hydrogen atoms (SHELXL-97).[35] Both programs were operated under the WinGX[36] program package. Hydrogen atoms attached to the C atoms of the bpy ligands were treated as riding in idealized positions, with C–H distances of 0.93 Å and displacement parameters assigned as $U_{iso}(H) = 1.2U_{eq}(C)$. Water molecules O22, O23 and O24 in **1** are disordered over two positions: O23a, O23b, O24a and O24b were fixed to equal occupancies of 0.5, while O22a has an occupancy of 0.68(7), and O22b an occupancy of 0.32(7). Some hydrogen atoms of the water molecules were recognized in the difference Fourier map, and some were determined using the M. Nardelli[37] algorithm implemented in the WinGX[36] program package. The O–H distances in all water molecules were restrained to a target value of 0.85(2) Å and an H–O–H angle of 104°.

The X-ray diffraction experiment on the single crystals of **3** was conducted several times at low temperature. Nevertheless, the data obtained were not satisfactory and the crystal structure of **3** could not be fully refined. The bulky constituent structural units, the one and a half $[\{Ni(bpy)_2\}_2(\mu\text{-}C_2O_4)]^{2+}$ cations and the $[TaO(C_2O_4)_3]^{3-}$anion, were recognized in the Fourier electron density map of **3**, whereas a large number of water molecules could not be exactly defined.

Geometrical calculations were carried out with PLATON[38] and the figures were made by the use of the ORTEP-3 (ref. 39) and MERCURY[40] programs. CCDC 1026178–1026180 contain the supplementary crystallographic data for this paper.

Acknowledgements

This research was supported by the Ministry of Science, Education and Sports of the Republic of Croatia (grant no. 098-0982904-2946 and 119-1193079-1084). The authors thank Dr. Krešimir Molčanov (RBI) for valuable discussions related to crystal structure refinement.

Notes and references

1 H. Okawa, A. Shigematsu, M. Sadakiyo, T. Miyagawa, K. Yoneda, M. Ohba and H. Kitagawa, *J. Am. Chem. Soc.*, 2009, **131**, 13516–13522.
2 M. Clemente-León, E. Coronado, C. Martí-Gastaldo and F. M. Romero, *Chem. Soc. Rev.*, 2011, **40**, 473–497.
3 I. Imaz, G. Bravic and J.-P. Sutter, *Dalton Trans.*, 2005, 2681–2687.
4 X.-L. Sun, B.-X. Shen, S.-Q. Zang and C.-X. Du, *CrystEngComm*, 2013, **15**, 5910–5918.
5 P. Thuéry and E. Rivière, *Dalton Trans.*, 2013, **42**, 10551–10558.
6 T. Grancha, C. Tourbillon, J. Ferrando-Soria, M. Julve, F. Lloret, J. Pasán, C. Ruiz-Pérez, O. Fabelo and E. Pardo, *CrystEngComm*, 2013, **15**, 9312–9315.
7 T. G. Prokhorova, L. V. Zorina, S. V. Simonov, V. N. Zverev, E. Canadell, R. P. Shibaeva and E. B. Yagubskii, *CrystEngComm*, 2013, **15**, 7048–7055.
8 Q. Pan, Q. Chen, W.-C. Song, T.-L. Hu and X.-H. Bu, *CrystEngComm*, 2010, **12**, 4198–4204.
9 M. Hernández-Molina, P. A. Lorenzo-Luis and C. Ruiz-Pérez, *CrystEngComm*, 2001, **3**, 60–63.
10 C. Janiak, *J. Chem. Soc., Dalton Trans.*, 2000, 3885–3896.
11 C. R. Martinez and B. L. Iverson, *Chem. Sci.*, 2012, **3**, 2191–2201.
12 I. Dance and M. Scudder, *CrystEngComm*, 2009, **11**, 2233–2247.
13 L. Androš, D. Matković-Čalogović and P. Planinić, *CrystEngComm*, 2013, **15**, 533–543.
14 Y.-L. Bai, J. Tao, R.-B. Huang and L.-S. Zheng, *CrystEngComm*, 2008, **10**, 472–474.
15 K. Latham, E. J. Mensforth, C. J. Rix and J. M. White, *CrystEngComm*, 2009, **11**, 1343–1351.
16 I. Katsuki, N. Matsumoto and M. Kojima, *Inorg. Chem.*, 2000, **39**, 3350–3354.
17 L. Pérez-García and D. B. Amabilino, *Chem. Soc. Rev.*, 2002, **31**, 342–356.
18 T. Tunyogi, A. Deák, G. Tárkányi, P. Király and G. Pálinkás, *Inorg. Chem.*, 2008, **47**, 2049–2055.
19 S. Khatua, H. Stoeckli-Evans, T. Harada, R. Kuroda and M. Bhattacharjee, *Inorg. Chem.*, 2006, **45**, 9619–9621.
20 L. Jiang, X.-L. Feng, C.-Y. Su, X.-M. Chen and T.-B. Lu, *Inorg. Chem.*, 2007, **46**, 2637–2644.
21 L. Androš, M. Jurić, J. Popović, A. Šantić, P. Lazić, M. Benčina, M. Valant, N. Brničević and P. Planinić, *Inorg. Chem.*, 2013, **52**, 14299–14308.
22 G. Mathern and R. Weiss, *Acta Crystallogr., Sect. B: Struct. Crystallogr. Cryst. Chem.*, 1971, **27**, 1610–1618.
23 M. Jurić, B. Perić, N. Brničević, P. Planinić, D. Pajić, K. Zadro, G. Giester and B. Kaitner, *Dalton Trans.*, 2008, 742–754.

24 M. Jurić, J. Popović, A. Šantić, K. Molčanov, N. Brničević and P. Planinić, *Inorg. Chem.*, 2013, **52**, 1832–1842.
25 J. Breu, W. Seidl, D. Huttner and F. Kraus, *Chem. – Eur. J.*, 2002, **8**, 4454–4460.
26 C. R. Groom and F. H. Allen, *Angew. Chem., Int. Ed.*, 2014, **53**, 662–671.
27 I. Dance and M. Scudder, *J. Chem. Soc., Dalton Trans.*, 1998, 1341–1350.
28 B. Jee, J. Zank, I. Dance, S. B. Wild, P. Klüfers and A. Willis, *CrystEngComm*, 2000, **35**, 1–5.
29 G. R. Lewis and I. Dance, *Inorg. Chim. Acta*, 2000, **306**, 160–167.
30 M. Scudder and I. Dance, *J. Chem. Soc., Dalton Trans.*, 1998, 3155–3165.
31 K. Nakamoto, *Infrared and Raman Spectra of Inorganic and Coordination Compounds*, John Wiley, New York, 6th edn, 2009.
32 L. Androš, M. Jurić, P. Planinić, D. Žilić, B. Rakvin and K. Molčanov, *Polyhedron*, 2010, **29**, 1291–1298.
33 *CrysAlis PRO*, Oxford Diffraction Ltd., UK, 2007.
34 A. Altomare, G. Cascarano, C. Giacovazzo and A. Guagliardi, *J. Appl. Crystallogr.*, 1993, **26**, 343–350.
35 G. M. Sheldrick, *Acta Crystallogr., Sect. A: Found. Crystallogr.*, 2008, **64**, 112–122.
36 L. J. Farrugia, *J. Appl. Crystallogr.*, 1999, **32**, 837–838.
37 M. Nardelli, *J. Appl. Crystallogr.*, 1999, **32**, 563–571.
38 L. Spek, *J. Appl. Crystallogr.*, 2003, **36**, 7–13.
39 L. J. Farrugia, *J. Appl. Crystallogr.*, 1997, **30**, 568.
40 F. Macrae, P. R. Edgington, P. McCabe, E. Pidcock, G. P. Shields, R. Taylor, M. Towler and J. van de Streek, *J. Appl. Crystallogr.*, 2006, **39**, 453–457.
41 H. D. Flack, *Acta Crystallogr., Sect. A: Found. Crystallogr.*, 1983, **39**, 876–881.